OPEN ACCESS
JOURNAL OF ADVANCED DIELECTRICS
Vol. 13, No. 6 (2023) 2345002 (6 pages)
© The Author(s)
DOI: 10.1142/S2010135X23450029

Analysis of multi-center topological domain states in $BiFeO_3$ nanodot arrays*

Zhongwen Li†,§, Siyi Zhang, Qingsheng Li and Hao Liu‡,§
Faculty of Mathematics and Physics, Huaiyin Institute of Technology
Huai'an, Jiangsu 223003, P. R. China
†lizhongwen@hyit.edu.cn
‡hyitliuh@163.com

Received 26 May 2023; Revised 20 June 2023; Accepted 26 June 2023; Published 14 July 2023

High-density ferroelectric $BiFeO_3$ (BFO) nanodot arrays were developed through template-assisted tailoring of epitaxial thin films. By combining piezoresponse force microscopy (PFM) and Kelvin probe force microscopy (KPFM) imaging techniques, we found that oxygen vacancies in nanodot arrays can be transported in the presence of an electric field. Besides triple-center domains, quadruple-center domains with different vertical polarizations were also identified. This was confirmed by combining the measurements of the domain switching and polarization vector distribution. The competition between the accumulation of mobile charges, such as oxygen vacancies, on the interface and the geometric constraints of nanodots led to the formation of these topological domain states. These abnormal multi-center topological defect states pave the way for improving the storage density of ferroelectric memory devices.

Keywords: Topological domains; oxygen vacancies; ferroelectric nanodot.

1. Introduction

Understanding chemical states is a key in revealing the physics of multiferroics at the nanoscale, be it their chemical (e.g., chemical bonds), mechanical (e.g., strain), or electrical (e.g., mobile charges and oxygen vacancies (V_Os)) properties.[1–15] In particular, V_Os have received attention in many aspects of emerging topological polar structures.[4,5] The most common of these is the two-dimensional (2D) topological ferroelectric domain walls, which are aggravated by the appearance of energetically costly head-to-head and tail-to-tail domain walls. These charged domain walls repel or attract V_Os, which in turn assist in stabilizing these topological defects.[16,17] In the past, studies have been primarily focused on the conductivity enhancement of these charged domain walls and their innovative applications in electronics.[18–22] However, these topological defects can have a positive impact on improving the performance of ferroelectric materials, for example, by introducing strange topological domain states to improve the ferroelectric storage density.[23,24] In order to meet the rapidly growing demand for miniaturized memory devices, it is necessary to understand and model V_Os to create new topological states to optimize the designs.[25–27] In the process of preparing rhombohedral $BiFeO_3$ (BFO) nanostructures with eight polarization variants through appropriate methods, poor screening of polarization without the top electrode, geometric constraints and V_Os are beneficial for the formation of topological defects.[28–30]

In this study, we focused on methods for quantitative experimental detection of singular domain structures in high-density nanodots. Over the past two decades, piezoresponse force microscopy (PFM) has become an essential instrument for characterizing ferroelectric behaviors, as it can image and control ferroelectric domains at high-resolutions (5–30 nm).[32] In PFM, the tip of a conducting atomic force microscope is placed as a mobile top electrode and an oscillating voltage is applied between the top and bottom electrode under the ferroelectric layer. PFM detects local displacements in ferroelectric samples caused by the converse piezoelectric effect during the surface scanning process. Domain images can be simultaneously obtained through vertical PFM (VPFM) and lateral PFM (LPFM) measurements which can determine the out-of-plane (OOP) and in-plane (IP) polarization components of the domain structures, respectively. The combination of the experimental data from one VPFM and two orthogonal LPFM scans to construct the full polarization vector is known as the vector PFM method.[31]

Several studies have determined the three-dimensional (3D) domain structure of bulk samples by thinning the medium and controlling the polarization distribution of the local surface.[24–26,30–32] These methods have revealed the structure and the unique properties of the exotic domains in nanoscale ferroelectrics, such as hexagonal $YMnO_3$, $PbTiO_3$/$SrTiO_3$ multilayer films and superlattices and BFO thin films and high-density nanodot arrays.[33–36] The effect of V_Os as

*This paper was originally submitted to the Special Issue on Ferroelectric Nanoelectronic Devices for Next-Generation Information Technology organized by Zheng Wen, Shuoguo Yuan, Zhen Fan and Yunya Liu.

§Corresponding authors.

This is an Open Access article published by World Scientific Publishing Company. It is distributed under the terms of the Creative Commons Attribution 4.0 (CC BY) License which permits use, distribution and reproduction in any medium, provided the original work is properly cited.

charged domain wall stabilizers has been studied through both experiments and simulations.[37] However, due to the high instability of charged domain walls, topological domain reconstruction in nanoscale ferroelectrics still faces technical challenges.[38]

In this report, we probed V_Os in epitaxial high-density nanodot arrays, experimentally observed the domain switching in the samples and analyzed the results of the domain structure. Apart from triple-center domains, quadruple-center domains were also identified in the images. The most important driving force for the formation of the center domains was the uneven distribution of V_Os.

2. Materials and Methods

In order to reduce crosstalk, the elements used to store data bits were physically separated to localize the electric field distribution. High-density BFO nanodot arrays were synthesized by ion-etching sacrificial nanoporous anodic aluminum oxide (AAO) templates.[23]

To characterize the surface, a Cypher S atomic force microscope (Asylum Research, USA) was used to perform PFM measurements in the dual AC resonance tracking (DART) mode, with a conductive tip coated with Platinum/Iridium. Moreover, the epitaxial structure was analyzed through X-ray diffraction (XRD, PANalytical X'Pert PRO) and scanning electron microscopy (SEM, Zeiss Ultra 55). Contact resonance frequencies of 260–300 kHz and 1 MHz were applied in the vertical and lateral orientations of the cantilever. A tip bias exceeding the coercive field was used to switch domains in the ferroelectric medium. During switching spectroscopy PFM (SS-PFM) measurements, local hysteresis loops were obtained at each image point to generate a 3D data array. The information about the coercive bias, imprint and switchable polarization was then extracted from this data.

3. Results

XRD patterns featured the (001) and (002) peaks from BFO, $SrRuO_3$ (SRO) and $SrTiO_3$ (STO) [Fig. 1(a)]. The OOP lattice constant was ~4.03 Å, close to that of rhombohedral BFO films. The SEM image [Fig. 1(b)] depicts the nanodot arrays on the STO substrate; the higher contrast areas between the nanodots indicated their physical separation. AFM measurement on a surface area of 0.6 μm^2 [Fig. 1(c)] revealed the well-ordered array of nanodots on the STO substrate. Nanodot arrays with a density of nearly 20 Gb $inch^{-2}$ had an average height of 20 nm and a lateral dimension of 60 nm (determined by measuring the half-maximum width of the nanodots) [Fig. 1(d)].

To detect V_Os, Kelvin probe force microscopy (KPFM) measurements were performed on a 0.8 μm × 0.8 μm surface of nanodot arrays [Fig. 2(e)]. KPFM is a noninvasive imaging technique to obtain the contact potential difference (CPD) between the probe and specimen surface. However,

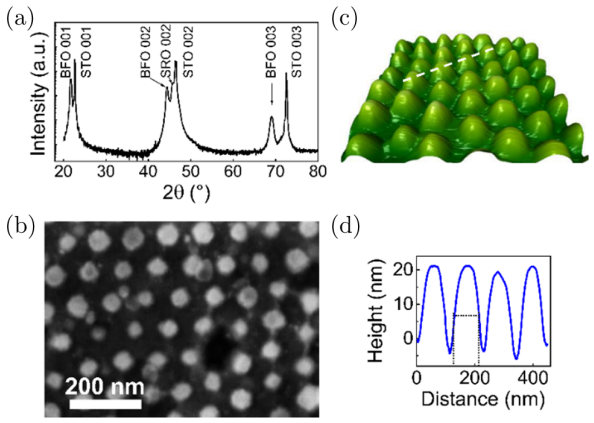

Fig. 1. Structure and atomic force microscopy (AFM) images of a BFO nanodot array. (a) XRD pattern, a.u., arbitrary units, (b) SEM image, (c) 3D AFM image and (d) height signal extracted from white dashed lines of the AFM image.

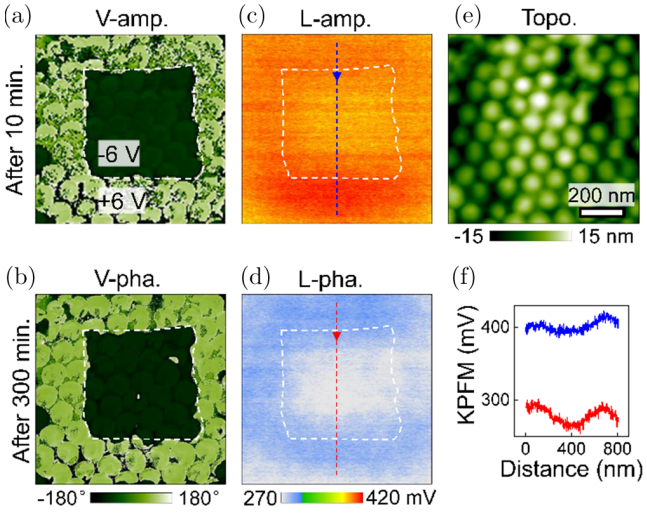

Fig. 2. (Color online) (a) and (b) VPFM (V-pha.) and (c) and (d) KPFM images of the nanodot array after poling with ±6 V tip bias for (a) and (c) 5 min and (b) and (d) 480 min; the polarized area is shown as the rectangle with a dark inner region and bright outer region. (e) Topography (Topo.) of the nanodot arrays. (f) KPFM signals were collected from the blue and red dashed lines in (c) and (d).

the presence of V_Os in the specimen surface, accumulated locally by electrical poling, can affect the CPD [Figs. 2(a) and 2(b)]. The KPFM images were taken 10 min and 300 min after the polarization [Figs. 2(c) and 2(d)]. The apparent contrasts of these images represent surface charging, either through hydroxyl/protons groups, injected charges, or V_Os.[4] However, since V_Os can recombine with oxygen through surface reaction or diffusion, the V_O concentration decreased with time, as inferred through a decrease in the contrast of KPFM images in polarized regions over time [Fig. 2(f)]. Therefore, it was speculated that V_Os are the origin of surface charge, which either diffuse or recombine with oxygen present in the environment.

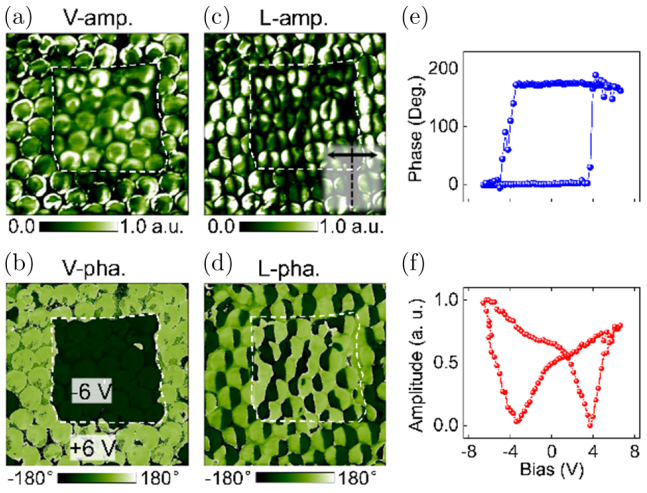

Fig. 3. Vectorial PFM images measured on 1.0 × 1.0 μm^2 nanodot arrays after poling with ±6 V tip bias. (a) VPFM amplitude (V-amp.) and (b) phase (V-pha). images. (c) LPFM amplitude (L-amp.) and (d) phase (L-pha.) images; The fast-scanning direction was parallel to the long axis of the probe cantilever in (c). (e) Phase and (f) amplitude of PFM hysteresis loops of a selected nanodot.

To determine the polarization direction, the domains in the nanodot array were polarized through a preset rectangular bias pattern (internal, –6 V; external, +6 V) and imaged using vector PFM [Figs. 3(a)–3(d)]. The dark (bright) regions [Fig. 3(b)] represented the domains with upward (downward) polarization as the negative (positive) tip bias generated an upward (downward) electric field. To prove the ferroelectricity of the sample and estimate the switching voltage required for domains, we carried out the SS-PFM measurements [Fig. 3(f)] and obtained the magnitude of the coercive field E_C to be ~3.7 V. The domain was difficult to flip and preferred its existing polarization, resulting in one polarization state being dominant compared to the other. This effect corresponds to the shift of the loop line [Fig. 3(e)] and the back switching of the domains in individual nanodots [Fig. 3(b)]. The 180° phase difference shown in the phase image [Fig. 3(e)] was consistent with the expected good ferroelectricity of the nanodots.

In this study, the contrasts of VPFM and LPFM phase (V-pha. and L-pha.) images were found to be one-to-one, i.e., the OOP vibration was displayed as a uniform dark (light) contrast and the IP vibrations were displayed as a left-dark/right-light (left-light/right-dark) contrast arrangement. There was a synchronous correspondence between the contrast of the VPFM and LPFM amplitude (V-amp. and L-amp.) images, which were both dark and light for a single nanodot. However, no correspondence was observed between the contrasts of the amplitude and phase images. For example, in the VPFM images, nanodots with a lighter contrast in the V-amp. image [Fig. 3(a)] had both dark and light contrasts in V-pha. image [Fig. 3(b)] and vice versa. The contrast distributions of the L-amp. [Fig. 3(c)] and L-pha. [Fig. 3(d)] images in the as-grown state were generally consistent with the above-mentioned case. Accordingly, the dark lines in the V-amp. images [Figs. 3(a) and 4(a)] with the minimum value mark the location of domain separation, i.e., domain walls.

The PFM images in Fig. 3 were analyzed to extract the components of polarization in the [100] (*x*-) and [001] (*z*-) axes. To fully determine the vector direction of polarization of a single nanodot in 3D space, complementary data of the [010] (*y*-) axis component also needs to be taken into account.[31] This was realized by rotating the sample and

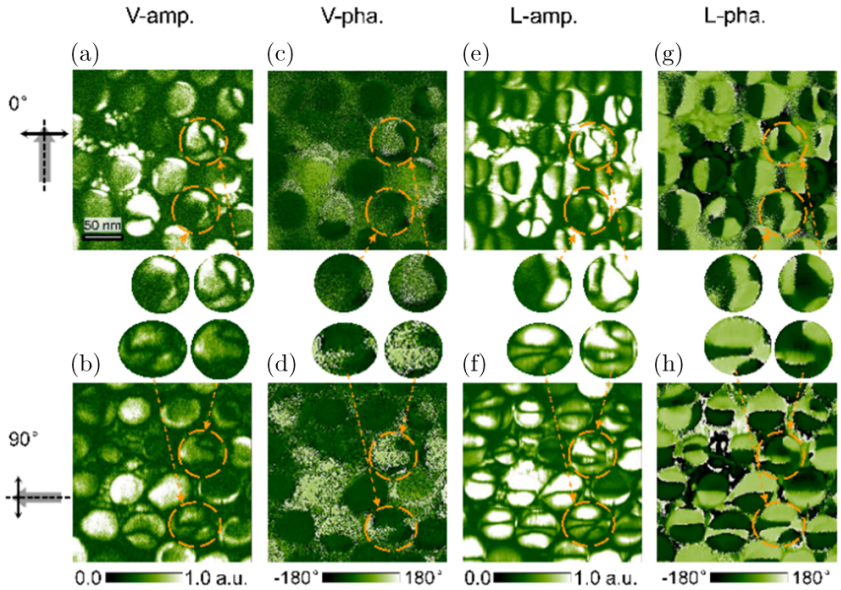

Fig. 4. Vector PFM: (a) and (b) V-amp. (c) and (d) V-pha. (e) and (f) L-amp. and (g) and (h) L-pha. images for different probe cantilever rotation angles: 0º (a, c, e, g) and 90° (b, d, f, h). The scale bars in (a) represent 50 nm.

recombining PFM data from the two orthogonal IP directions (Fig. 4). Figures 4(e) and 4(g) show the LPFM images (amplitude and phase) of the *x*-component (for cantilever rotation angle of 0°, i.e., parallel to [100]); Figs. 4(f) and 4(h) show the *y*-component (for cantilever rotation angle of 90°, i.e., parallel to [010]); and Figs. 4(a)–4(d) show the VPFM images of the *z*-component. Four types of domains were detected from the PFM images; a detailed description can be found in a previous study.[30] We chose the typical contrast of type IV PFM in the nanodot as an example because of its triple contrast distribution of OOP polarization (dark/light/dark). It was extracted from the nanodot arrays and amplified; a schematic representation of the reconstructed 3D polarization vector is shown in Fig. 5(i).

We identified the domain structure by overlaying the VPFM and LPFM images (Fig. 5); the enlarged images correspond to the nanodots marked in Fig. 4. First, the triple contrast (upper-left-light/upper-right-dark/lower-dark) in the V-pha. image [Fig. 5(a)] had a more complex contrast distribution in the two orthogonal L-pha. images [Figs. 5(c) and 5(e)]. Correspondingly, the dark lines in the V-amp. and L-amp. images (Fig. 4) mark the position of the wall separating the OOP and IP domains. These detections revealed a new phenomenon, highlighting the imminent issue of determining the polarization distribution in such domains. In the L-pha. images, the alternating light and dark contrasts represented the polarization direction, i.e., "left" or "right". This allowed us to establish a rule that the light and dark IP contrasts represent the left and right polarization components, respectively, relative to the long axis of the cantilever. Combining the IP 2D polarization distribution obtained from the above LPFM vector analysis with domain switching, we identified the typical topological domain states. Figures 5(a) and 5(b) show the triple contrast in the V-pha. image and multi-contrast sequences in the L-pha. image. Figure 5(g) shows the radial center-convergent, middle radial center-divergent and center-convergent domains with radial entad, ectad and entad polarization distributions, respectively. Similarly, Fig. 5(h) shows radial center-divergent, middle radial center-convergent and center-divergent domains with radial ectad, entad and ectad polarization distributions, respectively. Besides the triple-center domains, we also found the topological domain state with a quadruple-center [Fig. 6(f)]. We observed a quadruple contrast of light/dark/light/dark in the V-pha. image [Fig. 6(b)], while the homologous L-pha. image [Fig. 6(d)] had a more complicated contrast sequence. Correspondingly, the dark lines in the V-amp. [Fig. 6(a)] and L-amp. [Fig. 6(c)] images mark the position of the wall separating the OOP and IP domains. Interestingly, the intensity (R$\cos\theta$) [Fig. 6(e)] also had a relatively more complex contrast than the phase image [Fig. 6(d)]. These triple-center and quadruple-center type domain states were similar to the previously reported multi-center topological domains.[30] It is worth noting that the surface polarized charge was partially compensated as the multi-center domains contained both upward and downward polarizations. These center type topological domains are defined as a type of vortex.[39]

The charged domain wall (core) stabilized as charge carriers (V_Os) migrated freely to the charged core or domain head (tail). In addition, geometric constraints in low-dimensional nanomaterials play a vital role in the construction of topological domains. According to previous reports,

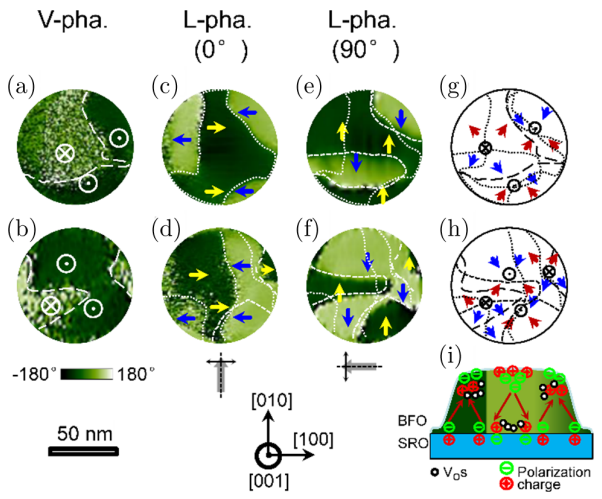

Fig. 5. Vector PFM images accompanied by the schematic diagram of triple-center states in nanodots: (a) and (b) V-pha. and (c)–(f) L-pha. images for different probe cantilever rotation angles: 0° (c, d) and 90° (e, f). (g) and (h) Schematic diagram of the top view of a multi-center domain structure obtained after 3D reconstruction of polarizations from the phase images. (i) Schematic diagram of the triple-center topological domain state induced by nonuniform charge enrichment.

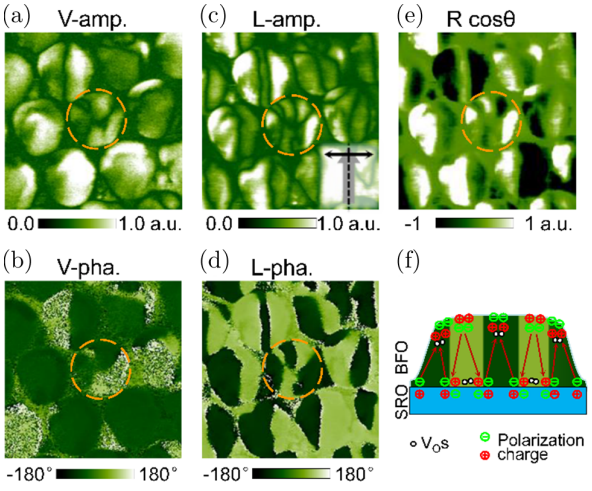

Fig. 6. Vectorial PFM images of a quadruple-center domain state. (a) V-amp., (b) V-pha., (c) L-amp., (d) L-pha. images and (e) combination of L-amp. (R) and L-pha. (θ) showing the intensity (R$\cos\theta$) of an as-grown nanodot sample. (f) Schematic diagram of the quadruple-center topological domain state. The fast-scanning direction was parallel to the long axis of the probe cantilever in (c).

phase-field simulations can be used to model the formation of topological structures in BFO nanoferroelectrics.[40] Due to the trapezoidal conical shape of the epitaxial BFO nanoparticles structure, the strain originating from the mismatch between the substrate and the nanodots gradually nullifies. Growth conditions and surface charges are the main factors affecting the evolution of domain states. On the top surface, the head-to-tail domain in the vortex structure can still result in no charged domain walls being formed without compensated charges, with the polarization roughly along the outer edge of the nanodots. If a relatively small surface charge gets accumulated in the center of the nanodots, a gradient electric field will be generated near the vortex core with receding field strength with distance. This gradient electric field causes a slight distortion extending from the vortex core. Compared to geometric constraints, the electric field strength increases with the accumulation of surface charges, gradually dominating the evolution of domain structures. Therefore, polarization is established along the direction of the electric field to construct a center-type domain. The dynamic process here is the competition and equilibration among the vortex structure produced by the surface charges and center-type domain.

Finally, the technological applications of these anomalous domains were examined. The center topological states were spontaneously generated during the growth of materials, indicating that they may be the most stable state, which is crucial for the control and operation of functional units. After 14 days of experimentation, most of the polarization domains observed in this study were stable under a normal air environment. The key to creating various types of topological defects (including center domain states and vortex states) are suggested to be the geometric parameters, V_Os and manufacturing techniques. By utilizing the top-down and bottom-up manufacturing strategies with a low-cost advantage, the required structures with a narrow size distribution can be produced on a large scale to easily obtain nanocapacitors < 100 nm. Therefore, in order to obtain smaller topological domains and higher information density, one can consider limiting the nanocapacitor to a smaller area to accumulate charges from the V_Os.

4. Conclusions

In summary, we demonstrated that V_Os can move in nanodot arrays under an electric field by combining KPFM and PFM imaging. Two unusual types of topological domain states were determined through the vector PFM analysis of the domain structures in BFO nanodot arrays, including triple-center and quadruple-center domain states with radial entad and ectad polarization arrangements. The stability of these center domains can be preserved by compensating the polarization charge with the accumulated charge. These findings indicate that the topological domain states are highly stable in discrete nanodots, and the key parameters controlling the size of the topological domains are the geometric parameters, V_Os, and manufacturing techniques.

Acknowledgments

This work was supported by the Natural Science Foundation of Huai'an (Grant No. HAB202150), Natural Science Foundation of the Jiangsu Higher Education Institutions of China (Grant No. 22KJD140002) and Jiangsu Students' Platform for Innovation and Entrepreneurship Training Program (Grant No. 202311049095Y).

References

[1]R. J. Zeches, M. D. Rossell, J. X. Zhang, A. J. Hatt, Q. He, C. H. Yang and R. Ramesh, A strain-driven morphotropic phase boundary in $BiFeO_3$, *Science* **326**, 977 (2009).
[2]D. Sando, A. Agbelele, D. Rahmedov, J. Liu, P. Rovillain, C. Toulouse and M. Bibes, Crafting the magnonic and spintronic response of $BiFeO_3$ films by epitaxial strain, *Nat. Mater.* **12**, 641 (2013).
[3]S. Dong, J.-M. Liu, S. W. Cheong and Z. Ren, Multiferroic materials and magnetoelectric physics: Symmetry, entanglement, excitation, and topology, *Adv. Phys.* **64**, 519 (2015).
[4]S. Das, B. Wang, Y. Cao, M. Rae Cho, Y. Jae Shin, S. Mo Yang, L. Wang, M. Kim, S. V. Kalinin, L.-Q. Chen and T. W. Noh, Controlled manipulation of oxygen vacancies using nanoscale flexoelectricity, *Nat. Commun.* **8**, 615 (2017).
[5]J. S. Lim, J. H. Lee, H. S. Park, R. Gao, T. Y. Koo, L. W. Martin and C. H. Yang, Ultrafast collective oxygen-vacancy flow in Ca-doped $BiFeO_3$, *NPG Asia Mater.* **10**, 943 (2018).
[6]G. Tian, W. Yang, D. Chen, Z. Fan, Z. Hou, M. Alexe and X. Gao, Topological domain states and magnetoelectric properties in multiferroic nanostructures, *Natl. Sci. Rev.* **6**, 684 (2019).
[7]C. Ahn, A. Cavalleri, A. Georges, S. Ismail-Beigi, A. J. Millis and J. M. Triscone, Designing and controlling the properties of transition metal oxide quantum materials, *Nat. Mater.* **20**, 1462 (2021).
[8]W. Yang, G. Tian, Y. Zhang, F. Xue, D. Zheng, L. Zhang, Y. Wang, C. Chen, Z. Fan, Z. Hou, D. Chen, J. Gao, M. Zeng, M. Qin, L.-Q. Chen, X. Gao and J.-M. Liu, Quasi-one-dimensional metallic conduction channels in exotic ferroelectric topological defects, *Nat. Commun.* **12**, 1306 (2021).
[9]Y. Wang, H. Wang, W. Tan and D. Huo, Magnetization reversal, critical behavior, and magnetocaloric effect in $NdMnO_3$: The role of magnetic ordering of Nd and Mn moments, *J. Appl. Phys*. **132**, 183907 (2022).
[10]Y. Wang, S. Ni, H. Zhang, H. Wang, K. Su, D. Yang, S. Huang, D. Huo and W. Tan, The negative magnetization and exchange bias effect in compound $NdMnO_3$: The role of magnetic ordering of Nd^{3+} and Mn^{3+} ions, *Appl. Phys. A* **128**, 839 (2022).
[11]A. N. Morozovska, E. A. Eliseev, A. Biswas, H. V. Shevliakova, N. V. Morozovsky and S. V. Kalinin, Chemical control of polarization in thin strained films of a multiaxial ferroelectric: Phase diagrams and polarization rotation, *Phys. Rev. B* **105**, 094112 (2022).
[12]H. B. Zhang, M. M. Yang and M. Alexe, Boosting the photocurrent in $BiFeO_3$ thin films via a domain-wall-defect interaction, *Adv. Photon. Res.* **4**, 2200189 (2023).
[13]Y. Yeo, S. Y. Hwang, J. Yeo, J. Kim, J. Jang, H. S. Park, Y.-J. Kim, D. D. Le, K. Song, M. Kim, S. Ryu, S.-Y. Choi and C. H. Yang, Configurable crack wall conduction in a complex oxide, *Nano Lett.* **23**, 398 (2023).
[14]Y. Wu, Y. Li, C. Zhou, H. Chen, S. W. Cheong, Y. Li, X. Tao and L. Zhang, Novel geometric ferroelectric $EuInO_3$ single crystals with topological vortex domains, *Cryst. Growth Des*. **23**, 1980 (2023).

[15]S. W. Cheong, M. Fiebig, W. Wu, L. Chapon and V. Kiryukhin, Seeing is believing: Visualization of antiferromagnetic domains, *NPJ Quantum Mater.* **5**, 3 (2020).
[16]J. Seidel, L. W. Martin, Q. He, Q. Zhan, Y.-H. Chu, A. Rother, M. E. Hawkridge, P. Maksymovych, P. Yu, M. Gajek, N. Balke, S. V. Kalinin, S. Gemming, F. Wang, G. Catalan, J. F. Scott, N. A. Spaldin, J. Orenstein and R. Ramesh, Conduction at domain walls in oxide multiferroics, *Nat. Mater.* **8**, 229 (2009).
[17]T. Rojac, A. Bencan, G. Drazic, N. Sakamoto, H. Ursic, B. Jancar and D. Damjanovic, Domain-wall conduction in ferroelectric $BiFeO_3$ controlled by accumulation of charged defects, *Nat. Mater.* **16**, 322 (2017).
[18]A. Crassous, T. Sluka, A. K. Tagantsev and N. Setter, Polarization charge as a reconfigurable quasi-dopant in ferroelectric thin films, *Nat. Nanotechnol.* **10**, 614 (2015).
[19]P. Li, Z. Huang, Z. Fan, H. Fan, Q. Luo, C. Chen, D. Chen, M. Zeng, M. Qin, Z. Zhang, X. Lu, X. Gao and J.-M. Liu, An unusual mechanism for negative differential resistance in ferroelectric nanocapacitors: Polarization switching-induced charge injection followed by charge trapping, *ACS Appl. Mater. Inter.* **9**, 27120 (2017).
[20]Z. W. Li, Z. Fan and G. F. Zhou, Nanoscale ring-shaped conduction channels with memristive behavior in $BiFeO_3$ nanodots, *Nanomaterials* **8**, 1031 (2018).
[21]D. Meier and S. M. Selbach, Ferroelectric domain walls for nanotechnology, *Nat. Rev. Mater.* **7**, 157 (2022).
[22]Z. Liu, H. Wang, M. Li, L. Tao, T. R. Paudel, H. Yu, Y. Wang, S. Hong, M. Zhang, Z. Ren, Y. Xie, E. Y. Tsymbal, J. Chen, Z. Zhang and H. Tian, In-plane charged domain walls with memristive behaviour in a ferroelectric film, *Nature* **613**, 656 (2023).
[23]Z. W. Li, Y. J. Wang, G. Tian, P. L. Li, L. Zhao, F. Y. Zhang, J. X. Yao, H. Fan, X. Song, D. Y. Chen, Z. Fan, M. H. Qin, M. Zeng, Z. Zhang, X. B. Lu, S. J. Hu, C. H. Lei, Q. F. Zhu, J. Y. Li, X. S. Gao and J.-M. Liu, High-density array of ferroelectric nanodots with robust and reversibly switchable topological domain states, *Sci. Adv.* **3**, e1700919 (2017).
[24]J. Ma, J. Ma, Q. H. Zhang, R. C. Peng, J. Wang, C. Liu, M. Wang, N. Li, M. F. Chen, X. X. Cheng, P. Gao, L. Gu, L. Q. Chen, P. Yu, J. X. Zhang and C. W. Nan, Controllable conductive readout in self-assembled, topologically confined ferroelectric domain walls, *Nat. Nanotechnol.* **13**, 947 (2018).
[25]G. F. Nataf, M. Guennou, J. M. Gregg, D. Meier, J. Hlinka, E. K. H. Salje and J. Kreisel, Domain-wall engineering and topological defects in ferroelectric and ferroelastic materials, *Nat. Rev. Phys.* **2**, 634 (2020).
[26]W. Yang, G. Tian, H. Fan,Y. Zhao, H. Chen, L. Zhang,Y. Wang, Z. Fan, Z. Hou, D. Chen, J. Gao, M. Zeng, X. Lu, M. Qin, X. Gao and J.-M. Liu, Nonvolatile ferroelectric-domain-wall memory embedded in a complex topological domain structure, *Adv. Mater.* **34**, 2107711 (2022).
[27]Z. W. Li, H. Shen, G. Dawson, Z. Zhang, Y. Wang, F. Nan, G. Song, G. Li, Y. Wu and H. Liu, Uniform arrays of centre-type topological domains in epitaxial ferroelectric thin films, *J. Mater. Chem. C* **10**, 3071 (2022).
[28]W. Peng, J. Mun, Q. Xie, J. Chen, L. Wang, M. Kim and T. W. Noh, Oxygen vacancy-induced topological nanodomains in ultrathin ferroelectric films, *NPJ Quantum Mater.* **6**, 48 (2021).
[29]Y. J. Wang, Y. L. Tang, Y. L. Zhu and X. L. Ma, Entangled polarizations in ferroelectrics: A focused review of polar topologies, *Acta Mater.* **243**, 118485 (2022).
[30]Z. W. Li, R. Bo, H. Shen, Y. Lin, G. Song, Y. Wang, G. Li, F. Nan, C. Wang, Y. Wu, Z. Zhang and H. Liu, Abnormal topological domains in a high-density array of ferroelectric nanodots, *J. Appl. Phys.* **133**, 094102 (2023).
[31]S. V. Kalinin, B. J. Rodriguez, S. Jesse, J. Shin, A. P. Baddorf, P. Gupta, H. Jain, D. B. Williams and A. Gruverman, Vector piezoresponse force microscopy, *Microsc. Microanal.* **12**, 206 (2006).
[32]A. Gruverman, M. Alexe and D. Meier, Piezoresponse force microscopy and nanoferroic phenomena, *Nat. Commun.* **10**, 1 (2019).
[33]L. Lu, Y. Nahas, Ming Liu, Hongchu Du, Z. Jiang, S. Ren, D, Wang, L. Jin, S. Prokhorenko, C. Jia and L. Bellaiche, Topological defects with distinct dipole configurations in $PbTiO_3/SrTiO_3$ multilayer films, *Phys. Rev. Lett.* **120**, 177601 (2018).
[34]S. Das, Z. Hong, M. Mccarter, P. Shafer, Y. T. Shao, D. A. Muller, L. W. Martin and R. Ramesh, A new era in ferroelectrics, *APL Mater.* **8**, 120902 (2020).
[35]K. P. Kelley, A. N. Morozovska, E. A. Eliseev, V. Sharma, D. E. Yilmaz, A. C. T. van Duin, P. Ganesh, A. Borisevich, S. Jesse, P. Maksymovych, N. Balke, S. V. Kalinin and R. K. Vasudevan, Oxygen vacancy injection as a pathway to enhancing electromechanical response in ferroelectrics, *Adv. Mater.* **34**, 2106426 (2022).
[36]Z. W. Li, S. Zhang, X. Li, Y. Wu, H. Wang and H. Liu, Center-type topological domain states in ferroelectric nanodots tailored from thin films, *Phys. Status Solidi RRL* **17**, 2200424 (2023).
[37]P. S. Bednyakov, B. I. Sturman, T. Sluka, A. K. Tagantsev and P. V. Yudin, Physics and applications of charged domain walls, *NPJ Comput. Mater.* **4**, 65 (2018).
[38]J. Junquera, Y. Nahas, S. Prokhorenko, L. Bellaiche, J. Íñiguez, D. Schlom, L.-Q. Chen, S. Salahuddin, D. A. Muller, L. W. Martin and R. Ramesh, Topological phases in polar oxide nanostructures, *Rev. Mod. Phys.* **95**, 2 (2023).
[39]D. Liu, X. Shi, J. Wang, X. Cheng and H. Huang, Phase-field simulations of surface charge-induced ferroelectric vortex, *J. Phys. D. Appl. Phys.* **54**, 405302 (2021).
[40]N. D. Mermin, The topological theory of defects in ordered media, *Rev. Mod. Phys.* **51**, 591 (1979).